Factors controlling sea salt modification and dry deposition of nonsea-salt components to the ocean

N. Kawakami,[1,2] K. Osada,[1] C. Nishita,[1] M. Yabuki,[3] H. Kobayashi,[4] K. Hara,[5] and M. Shiobara[3]

Received 21 September 2007; revised 29 January 2008; accepted 11 March 2008; published 29 July 2008.

[1] Modification of sea salt aerosol particles (SSA particles) by HNO_3 and SO_2 is an important process for changing phase partitioning of acidic gases from industrial regions to the ocean. During 12–29 September 2005, size-segregated aerosol particles and acidic gases were sampled around the western part of the Japanese Islands to elucidate controlling factors of modification of SSA particles by acidic gases and to estimate dry deposition flux over the ocean. For coarse (>2 μm diameter) SSA particles, the amount of Cl^- deficiency from the seawater ratio was comparable to the sum of the equivalent concentrations of NO_3^- and nonsea-salt (nss) SO_4^{2-}, suggesting Cl^- displacement of SSA particles by acidic gases such as HNO_3 and SO_2. The Cl^- deficiency of SSA particles varied according to the size range and wind speed. Decreasing modification occurred with increasing wind speed for particles of 2–8 μm. Under high (low) wind conditions, the NO_3^- concentration per unit surface area of coarse SSA particles was lower (higher) for particles >8 μm than for those of 2–8 μm diameter. The respective dry deposition fluxes (F_{dry}) of NO_3^-, nss-SO_4^{2-}, HNO_3, and SO_2 were estimated according to the wind speed and size of aerosol particles. On average, the F_{dry} of particulate NO_3^- was 10 times larger than that of HNO_3, but F_{dry} of nss-SO_4^{2-} was almost equal to that of SO_2. Phase partitioning of dry deposition for NO_3^- and nss-SO_4^{2-} over the ocean differs from that of coastal marine areas.

Citation: Kawakami, N., K. Osada, C. Nishita, M. Yabuki, H. Kobayashi, K. Hara, and M. Shiobara (2008), Factors controlling sea salt modification and dry deposition of nonsea-salt components to the ocean, *J. Geophys. Res.*, *113*, D14216, doi:10.1029/2007JD009410.

1. Introduction

[2] Sea salt aerosol particles derived from the ocean constitute the major component of the total aerosol mass in the lower atmosphere [*Andreae*, 1995]. Sea salt aerosol particles (SSA particles) are often modified by various acidic gases such as HNO_3 and SO_2 [*Okada et al.*, 1978; *Parungo et al.*, 1986; *Mamane and Mehler*, 1987; *McInnes et al.*, 1994; *Pósfai et al.*, 1995; *Pio and Lopes*, 1998; *Buseck and Pósfai*, 1999; *Hara et al.*, 1999; *Zhuang et al.*, 1999; *Spokes et al.*, 2000; *Rossi*, 2003]. Because supermicrometer SSA particles are quickly deposited onto the Earth's surface or are returned to the ocean, once they are absorbed and react with acidic gases, they carry nonsea-salt (nss) components, such as NO_3^- and nss-SO_4^{2-}, from the atmosphere to Earth's surface. The importance of supermicrometer SSA particles for dry deposition of NO_3^- and nss-SO_4^{2-} to the sea surface has been underscored in many reports such as those by *Sievering et al.* [1989], *Pryor and Sørensen* [2000], *Spokes et al.* [2000], *Yeatman et al.* [2001], *Russell et al.* [2003], and *Fischer et al.* [2006].

[3] Anthropogenic input of NO_3^- as a nutrient to coastal marine ecosystems might cause algal blooms and contribute to eutrophication [*Zhang*, 1994; *Paerl*, 1997]. For that reason, quantifying atmospheric NO_3^- flux to the ocean is an important task for studying eutrophication and developing a model to predict future scenarios [*Pryor and Sørensen*, 2002]. On the other hand, NO_x emissions, and therefore NO_2 concentrations, are increasing because of economic growth, especially in Asia [*Galloway and Cowlling*, 2002; *Akimoto*, 2003; *Richter et al.*, 2005; *van der A et al.*, 2006; *He et al.*, 2007; *Ohara et al.*, 2007; *Uno et al.*, 2007]. Because increased NO_x emissions might enrich HNO_3 in the coastal atmosphere in Asia, they might engender increased dry deposition flux of modified SSA particles by NO_3^-. Although the importance of dry deposition of aerosol phase NO_3^- to the sea surface has been studied in coastal marine areas near polluted cities [*Russell et al.*, 2003; *Nakamura et al.*, 2005; *Chen et al.*, 2007], wind speed dependence on the dry deposition velocity has not been considered for calculating the deposition flux of SSA particles.

[1] Graduate School of Environmental Studies, Nagoya University, Nagoya, Japan.
[2] Now at Aichi Environmental Research Center, Nagoya, Japan.
[3] National Institute of Polar Research, Itabashi, Japan.
[4] Interdisciplinary Graduate School of Medicine and Engineering, University of Yamanashi, Kofu, Japan.
[5] Faculty of Science, Fukuoka University, Fukuoka, Japan.

0148-0227/08/2007JD009410

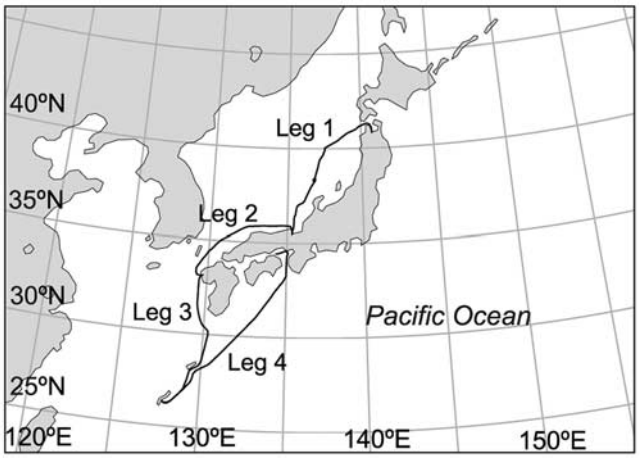

Figure 1. Cruise tracks of Legs 1–4 of the JARE 47 Training Cruise of the R/V *Shirase* during 12–29 September 2005.

[4] Dry deposition flux of aerosol particles to the ocean is usually calculated using the atmospheric concentration and deposition velocity of particles. For simplicity, data from previous reports of dry deposition flux of NO_3^- have used a fixed dry deposition velocity (such as 0.3 or 2 cm/s for coarse mode SSA particles) [*Duce et al.*, 1991; *Yeatman et al.*, 2001; *Nakamura et al.*, 2005]. Nevertheless, in reality, the dry deposition velocity increases not only with increasing SSA particle diameter, but also with wind speed [*Slinn and Slinn*, 1980; *Lewis and Schwartz*, 2004]. A multiplier effect of size and wind speed on the dry deposition velocity might be a source of large error in estimating the dry deposition flux for NO_3^- in coarse (>2 μm diameter) SSA particles. To obtain precise estimates of the dry deposition flux of NO_3^- associated with SSA particles, the size distribution of NO_3^- and its formation processes in supermicrometer aerosols must be studied in greater detail in relation to meteorological and gaseous conditions.

[5] For this study, we obtained size-segregated NO_3^- and nss-SO_4^{2-} concentrations in aerosol particles as well as acidic gaseous data for 12 h intervals to estimate the dry deposition fluxes over the open ocean of the western area of the Japanese archipelago. We discuss these concentration data with backward air trajectories and wind speed to explore the factors that control the size-dependent modification of coarse SSA particles with HNO_3 and SO_2. Finally, dry deposition fluxes of NO_3^- and nss-SO_4^{2-} are estimated using the dry deposition model described by *Lewis and Schwartz* [2004]; they are then compared to gaseous deposition fluxes.

2. Experiments and Supporting Data

2.1. Sampling and Experiments

[6] Size-segregated aerosol particles and water-soluble gases were sampled on board the R/V *Shirase* during 12–29 September 2005. Figure 1 shows the cruise tracks of Legs 1–4 of that cruise of the R/V *Shirase* during the study period. Aerosol particles were collected using a three-stage impactor with a back-up filter following a series of four-stage double alkaline and double acid impregnated filters for 12 h intervals (ca. 14 m^3 per sample). The air sampler was placed in a weather shield on the center-front end of the upper-most deck at 20 m above sea level. To prevent contamination from the ship's boundary layer, the inlet of the weather shield was designed to protrude toward the bow from the edge of the upper-most deck. That arrangement was determined based on measurements using a handheld condensation nucleus counter (3007; TSI Inc.). The inlet of the weather shield has a downward-facing cross-section of 240 (width perpendicular to long axis of the ship) × 50 (shorter length of the inlet) mm. The upper limit for passing the inlet into the weather shield is difficult to estimate because of the variety of wind conditions [e.g., *Mark*, 1998]. The aspiration efficiency (E_a) of the inlet airflow at various angles (45–90°) relative to the wind direction was estimated using the following equation [*Hangal and Willeke*, 1990]:

$$E_a = 1 + (\cos\theta - 1)\left(3Stk^{R^{-0.5}}\right), \quad (1)$$

where θ represents the angle of the inlet relative to the wind direction, *Stk* denotes the Stokes number, and *R* is the flow speed ratio of the inlet. Assuming wind speed of 10 m/s, 1.2 g/cm^3 particle density at 80% RH [*Tang et al.*, 1997], and *R* of 1, 15 μm is the diameter inferred to yield 50% efficiency for entering the inlet. Although the upper limit of the entering size must be highly variable with wind speed at the sampling, we will use this value as the best guess for the upper limit.

[7] The 50% cut off diameter (d_{50}) for the three-stage impactor can be estimated using the following equation [*Hinds*, 1999],

$$d_{50} = \sqrt{\frac{9\pi Stk_{50}\mu D_j^3}{4\rho_p Q C_c}}, \quad (2)$$

where Stk_{50} (0.24) is the Stokes number for 50% collection efficiency, μ is the viscosity coefficient of air (1.8×10^{-5} Pas at 20°C), D_j is the diameter of nozzles (Stage 1, 4; Stage 2, 1.6; Stage 3, 0.4 mm), *Q* is the airflow rate (m^3/s), and C_c is the Cunningham correction factor. The impactor used has 12, 7, and 19 nozzles for Stage 1, Stage 2, and Stage 3, respectively. The estimated 50% cutoff diameter is 8 μm for Stage 1, 2 μm for Stage 2, and 0.2 μm for Stage 3 at a flow rate of 20 L min^{-1}. Air sampling was controlled according to the relative wind speed (>2 m/s) and direction to avoid contamination from the ship's exhaust: sampling was limited to winds from the bow. The substrate of the first stage of the impactor was a PTFE filter (47 mm diameter; Advantec Toyo Kaisha Ltd.) with a 15 mm diameter hole at the center. Nucleopore filters (25 mm diameter; Whatman Japan K.K.) were used as sampling substrates for the second and third stages of the impactor. The back-up filter was a 47-mm-diameter PTFE filter (nominal pore size of 1.0 μm; Advantec Toyo Kaisha Ltd.). Acidic gases were collected using two alkaline-impregnated filters (1% Na_2CO_3 with 1% glycerol in methanol by mass). The sample airflow rate was measured using a mass flowmeter (SEF-51; Horiba STEC Co. Ltd.) that had been calibrated for standard temperature and pressure conditions (0°C and 1013 hPa).

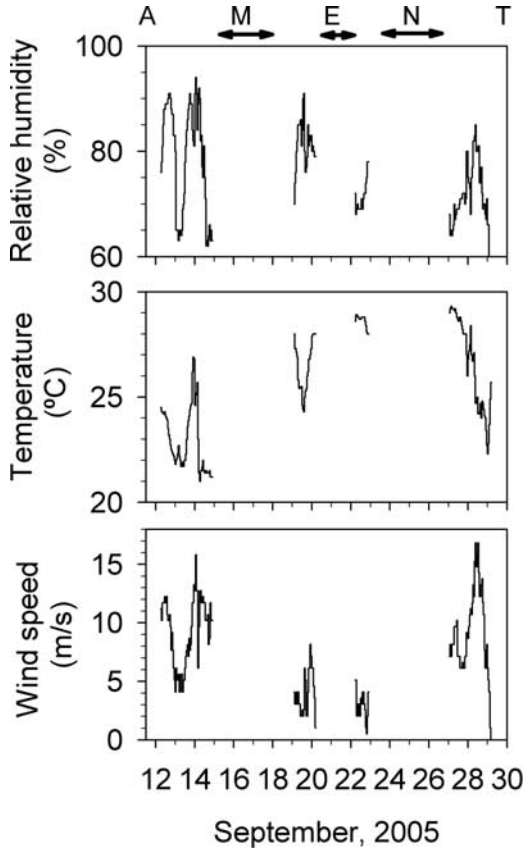

Figure 2. Hourly data of relative humidity, air temperature, and wind speed during the observation period of Legs 1–4. Air samples were not collected while the ship was anchored in ports at Aomori (A), Maizuru (M), Ebisu (E), Nakagusuku (N), and Takamatsu (T), shown at the top of the figure.

After the sampling, each filter was stored in a precleaned polypropylene 15 mL centrifuge vial with an airtight cap (Iwaki Glass Co. Ltd.), packed in polyethylene bags, and kept in a freezer until laboratory analyses.

[8] For extraction of water-soluble components from the aerosol filter sample, 10 mL of ultra-pure water (18 MΩ, Milli-Q water; Millipore Corp.) was added to the sample vial and immersed for 24 h. For analysis of acidic gases, 10.3 mL of 0.1% H_2O_2 solution was used. Ionic concentrations of water-soluble components in these samples were analyzed using ion chromatography [*Hara et al.*, 1999; *Osada et al.*, 2007]. The analyzed ions were F^-, CH_3COO^-, $HCOO^-$, $CH_3SO_3^-$, Cl^-, Br^-, NO_3^-, SO_4^{2-}, and $C_2O_4^{2-}$ for anions, and Na^+, NH_4^+, K^+, Mg^{2+}, and Ca^{2+} for cations. We obtained several procedural blank samples during the observation period to evaluate possible contamination through sample handling and storage. Procedural blank samples were treated identically to actual aerosol samples without passing air into the filters. Concentrations of procedural blanks were mostly negligible but, when present, they were subtracted from the values in the actual sample. Sea salt (ss) and nonsea-salt (nss) concentrations were estimated from Na^+ concentrations in the samples using the bulk seawater ratios described by *Wilson* [1975].

2.2. Estimate of Dry Deposition Flux

[9] The dry deposition flux of particulate ($F_{\text{dry-}p}$) and gaseous ($F_{\text{dry-}g}$) species to the ocean surface is given by the product of the measured concentration (C) of the particles or gases in air and the deposition velocity (V_{dry}).

$$F_{\text{dry}} = V_{\text{dry}} C \tag{3}$$

To determine the size-dependent deposition flux of aerosol particles to the ocean surface, the dry deposition velocity for aerosol particles ($V_{\text{dry-}p}$) was estimated as a function of the wind speed and the geometric mean diameter of the sampling size range following *Lewis and Schwartz* [2004], which is a modified model of *Slinn and Slinn* [1980]. For determination of the size dependent dry deposition velocity, mechanisms that operate to transport SSA particles (gravitational sedimentation, turbulent diffusion, Brownian diffusion, and impaction on the sea surface) are parameterized by transport velocities that depend strongly on the particle size and on wind speed [*Lewis and Schwartz*, 2004]. The $V_{\text{dry-}p}$ of coarse SSA particles is expected to increase with increasing diameter because of the contribution from gravitational sedimentation. Additionally, $V_{\text{dry-}p}$ is expected to increase with increasing wind speed because of stronger vertical mixing of the surface layer and faster inertial impaction velocity. In this study, we used the wind speed measured at 25 m height, and 0.0013 for the wind stress coefficient [*Lewis and Schwartz*, 2004, p. 40]. Using an upper limit (15 μm) assumed for passing the inlet and 50% cutoff diameters of the cascade impactor (8, 2, and 0.2 μm) for average RH (80%) during the observation, the geometric mean diameters of the size ranges were estimated respectively as 11, 4, and 0.6 μm. Dry deposition flux for HNO_3 and SO_2 ($V_{\text{dry-}g}$) to the ocean were also estimated as a function of wind speed according to *Lindfors et al.* [1993].

3. Results and Discussion

3.1. Meteorological Conditions and Backward Air Trajectory

[10] Figure 2 presents hourly data of relative humidity, air temperature, and wind speed during the observation period of Legs 1–4 of the cruise. Air samples were not collected when the ship was anchored in ports at Aomori (A), Maizuru (M), Ebisu (E), Nakagusuku (N), and Takamatsu (T), as noted at the top of Figure 2. Rain occurred on 12, 13, 14, and 28 September. Wind speeds were high on 12, 14, and 28 September, mostly corresponding to those rainy periods. The average values of relative humidity, temperature, and wind speed were, respectively, 76%, 25°C, and 7.3 m/s.

[11] Figure 3 shows the 5-d backward air trajectories starting from 500 m and 1000 m above sea level at the midpoint of the sampling duration (HYSPLIT 4 [*Draxler and Rolph*, 2003]). Numbers with the trajectory indicate the sample identification used in later discussion. According to lidar measurements around Japan [*Sugimoto et al.*, 2002], the boundary layer height was up to 600–1500 m. For that reason, the air over the sea surface might be mixed up to 600–1500 m altitudes. Most trajectories show a similar movement for both altitudes. The air trajectories for samples 1–3, 5, and 7 were derived from the Pacific Ocean as a clockwise movement to the sampling sites in the Sea of

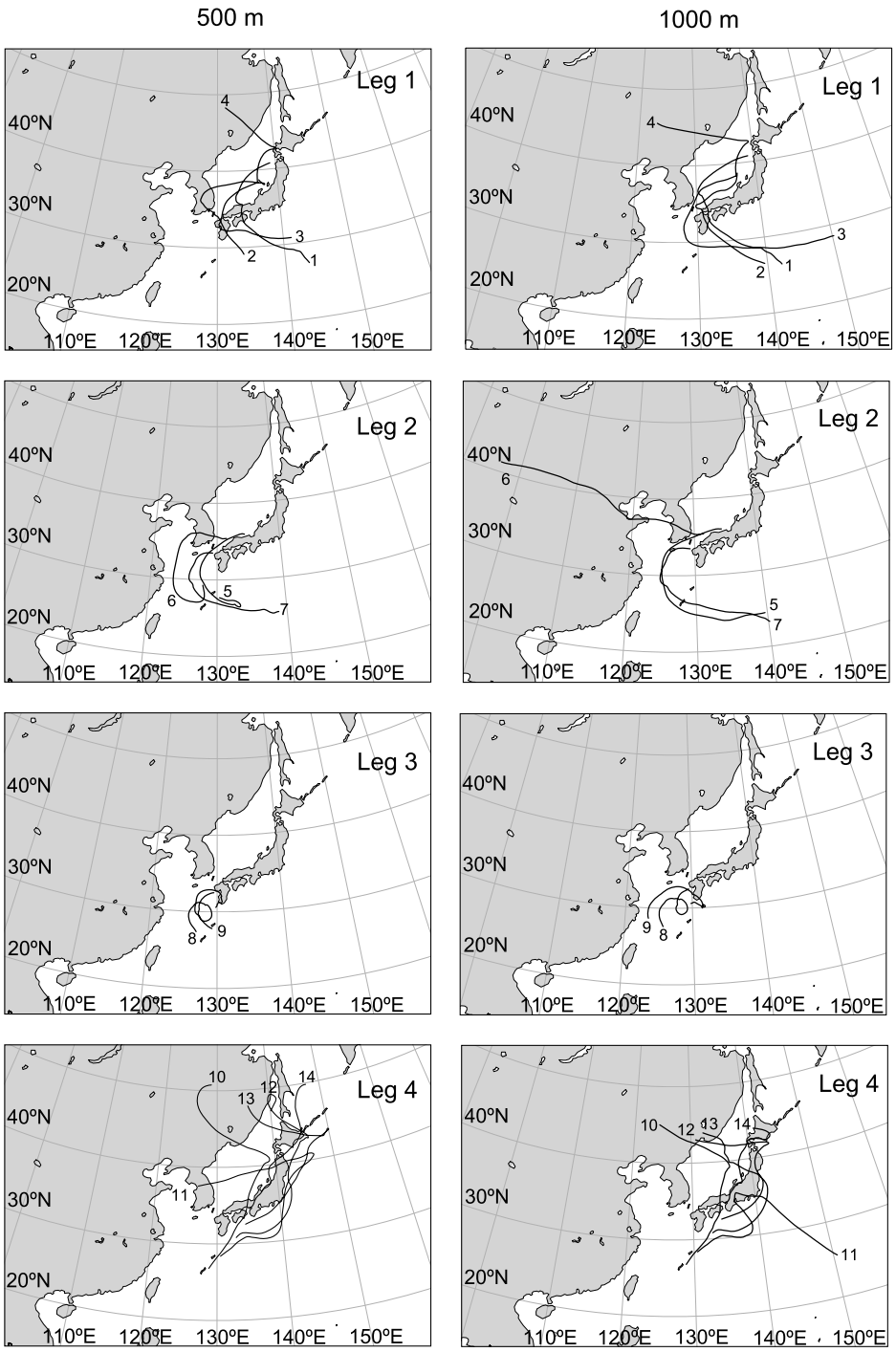

Figure 3. Five-day backward air trajectories starting from 500 m (left column) and 1000 m (right column) above sea level at the midpoint of sampling duration (HYSPLIT 4 [*Draxler and Rolph*, 2003]) for Legs 1–4. Numbers with trajectories indicate sample identification used in later discussion.

Japan. The air trajectory of sample 6, starting from 1000 m altitude, was derived from continental areas of China, which is separate from the trajectory of 500 m around the west of the Korean Peninsula. The air trajectories of samples 8–9 and 10–14 passed respectively over the East China Sea and around the Japanese Islands. The air trajectories of sample 11 were deviated from about 2 d before arrival. Most 5-d backward air trajectories were derived within 2000 km or much closer to the sampling site, except for sample 6, which was partly transported from inland China.

3.2. Ionic Concentrations of Aerosols and Acidic Gases

[12] Figures 4a–4f show size-segregated ionic concentrations (nmol/m^3) in aerosols during 12–29 September

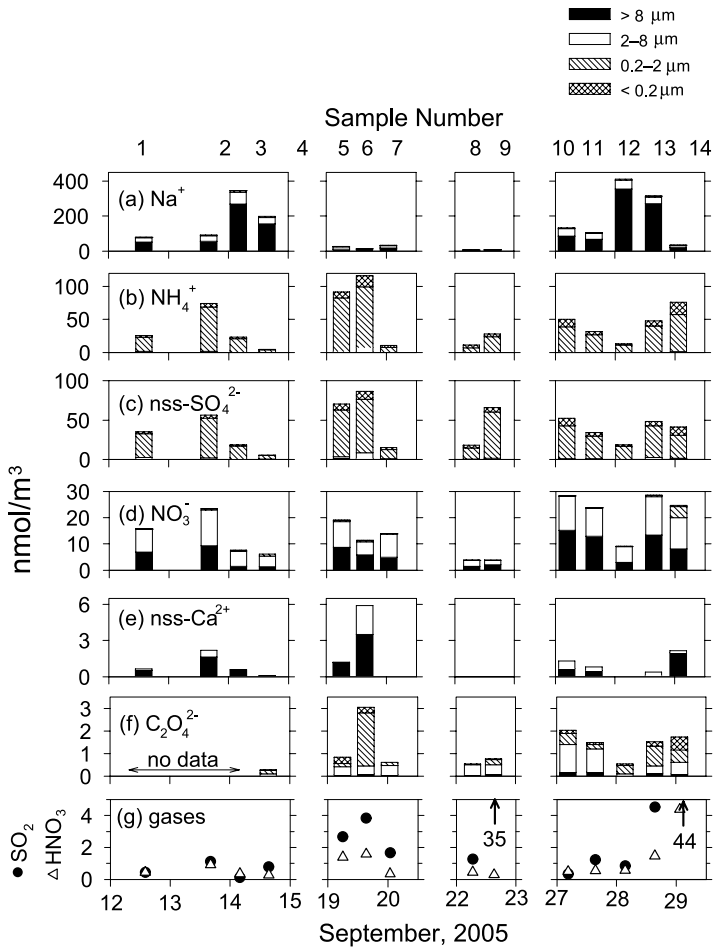

Figure 4. Size-segregated ionic concentrations in aerosols and acid gases during 12−29 September 2005 in nanomoles per cubic meter. Numbers at the top of the figure correspond to the sample numbers shown in Figure 3 and Table 1.

2005. Table 1 lists chemical and meteorological data. Numbers at the top of Figure 4a correspond to the sample numbers in Figure 3 and subsequent figures. In coarse particles with >2 μm diameter, Na^+, NO_3^- and nonsea-salt (nss) Ca^{2+} (also Cl^- and Mg^{2+}, both not shown) concentrations were found predominantly. In contrast, NH_4^+ and nss-SO_4^{2-} concentrations were dominant in fine (<2 μm) particles. The size distribution of $C_2O_4^{2-}$ was not readily calculable: the fine particles were dominant for sample 6, but the coarse particles dominated samples 10 and 11. Among ionic constituents in coarse particles, Na^+ and Cl^- were the dominant components. As discussed later in section 3.3.1, most coarse particles obtained in this study are considered as SSA particles. The Na^+ concentration was high in samples 3, 4, 12, and 13, which were obtained under strong wind conditions.

[13] Concentrations of nss-Ca^{2+}, $C_2O_4^{2-}$, NH_4^+, and nss-SO_4^{2-} were high in sample 6. The backward air trajectory for sample 6 started at 1000 m was derived from inland China, where high concentrations of Asian dusts and anthropogenic pollutants often occur [*Streets et al.*, 2003; *Osada et al.*, 2007]. High concentrations of these constituents in sample 6 are expected to be consistent with transport from such sources. Because ionic data of sample 6 might not represent the oceanic situation, we will not include data of sample 6 in later analyses of modifications of SSA particles.

[14] Figure 4g depicts atmospheric concentrations of HNO_3 and SO_2. Although SO_2 concentrations were almost identical to those of HNO_3 for samples 1, 3, and 10, the SO_2 concentrations were higher than those of HNO_3 for the remaining samples. In sample 9, both SO_2 and nss-SO_4^{2-} concentrations were high. According to the backward air trajectory, volcanic emissions of SO_2 and subsequent nss-SO_4^{2-} from Mt. Sakurajima on Kyushu Island [*Fujita et al.*, 1992] might have contributed matter to sample 9. The highest concentrations of HNO_3 and SO_2 were indicated for sample 14. The nss-SO_4^{2-}, NH_4^+, and $C_2O_4^{2-}$ in particles with <0.2 μm, and NO_3^- in particles with 0.2−2 μm diameter were also highest for sample 14. Considering that sample 14 was obtained from the anthropogenically polluted Seto Inland Sea area and that its trajectory passed over Japan mainland area, sample 14 is presumably influenced by local anthropogenic pollution in Japan. These general tendencies of concentration levels over the ocean around

Table 1. Chemical and Meteorological Data Observed During 12–29 September 2005[a]

SN	Leg	Time	WS, m/s	Temp., °C	RH, %	$[HNO_3]$ nmol/m^3	$[SO_2]$ nmol/m^3	Concentrations, nmol/m^3 Size Range, μm	<0.2	0.2–2	2–8	>8	A, mm^2/m^3 2–8	>8
1	1	12 Sep 6:00–22:10	10.6	23.6	87	0.4	0.4	$[Na^+]$	0.1	2.8	24.2	51.1	9.9	7.6
								$[Mg^{2+}]$	0.0	0.2	2.9	6.2		
								$[NH_4^+]$	2.4	21.9	1.0	0.5		
								$[Cl^-]$	0.1	0.1	15.7	49.8		
								$[NO_3^-]$	0.0	0.1	8.7	6.9		
								$[nss\text{-}SO_4^{2-}]$	2.5	30.4	2.0	0.4		
2	1	13 Sep 9:29–22:44	7.7	23.7	82	0.9	1.1	$[Na^+]$	0.1	4.3	33.2	54.8	13.6	8.1
								$[Mg^{2+}]$	0.0	0.3	3.9	6.8		
								$[NH_4^+]$	5.1	67.7	0.8	0.6		
								$[Cl^-]$	0.1	0.2	21.5	55.0		
								$[NO_3^-]$	0.1	0.4	13.6	9.3		
								$[nss\text{-}SO_4^{2-}]$	4.0	50.0	2.1	0.0		
3	1	13 Sep 22:50–14 Sep 8:57	12.0	23.6	88	0.4	0.1	$[Na^+]$	0.4	8.7	67.5	269	27.6	40.0
								$[Mg^{2+}]$	0.0	0.5	7.0	32.7		
								$[NH_4^+]$	2.3	20.6	0.0	0.0		
								$[Cl^-]$	0.6	1.0	70.0	304		
								$[NO_3^-]$	0.1	0.4	5.8	1.4		
								$[nss\text{-}SO_4^{2-}]$	1.4	16.8	0.4	0.0		
4	1	14 Sep 9:04–21:48	10.6	21.5	68	0.3	0.8	$[Na^+]$	0.3	5.7	36.9	155	15.1	23.0
								$[Mg^{2+}]$	0.0	0.4	3.8	17.5		
								$[NH_4^+]$	1.0	3.7	0.0	0.0		
								$[Cl^-]$	0.4	1.4	36.5	172		
								$[NO_3^-]$	0.0	0.6	4.1	1.3		
								$[nss\text{-}SO_4^{2-}]$	0.6	4.7	0.5	0.0		
5	2	19 Sep 2:00–9:56	3.4	26.7	80	1.4	2.7	$[Na^+]$	0.3	3.4	12.5	10.2	5.1	1.5
								$[Mg^{2+}]$	0.0	0.0	1.3	1.2		
								$[NH_4^+]$	9.4	80.7	0.5	1.1		
								$[Cl^-]$	0.1	0.1	2.2	5.5		
								$[NO_3^-]$	0.1	0.5	9.8	8.7		
								$[nss\text{-}SO_4^{2-}]$	7.4	59.3	2.1	1.4		
6	2	19 Sep 10:11–20:26	3.1	25.2	83	1.6	3.8	$[Na^+]$	0.5	1.5	5.4	5.1	2.2	0.8
								$[Mg^{2+}]$	0.0	0.3	1.2	0.9		
								$[NH_4^+]$	16.9	91.7	6.4	1.1		
								$[Cl^-]$	0.6	0.1	0.9	2.8		
								$[NO_3^-]$	0.1	0.5	5.0	5.9		
								$[nss\text{-}SO_4^{2-}]$	10.2	67.5	6.9	1.8		
7	2	19 Sep 20:43–20 Sep 4:58	5.4	27.5	81	0.4	1.7	$[Na^+]$	0.0	1.5	14.3	16.9	5.8	2.5
								$[Mg^{2+}]$	0.0	0.0	1.5	2.0		
								$[NH_4^+]$	2.5	7.8	0.0	0.0		
								$[Cl^-]$	0.1	0.0	6.1	15.1		
								$[NO_3^-]$	0.0	0.0	8.9	4.9		
								$[nss\text{-}SO_4^{2-}]$	2.6	11.6	0.5	0.3		
8	3	22 Sep 4:39–8:38	3.8	28.8	70	0.5	1.3	$[Na^+]$	0.4	0.3	2.9	2.8	1.2	0.4
								$[Mg^{2+}]$	0.0	0.0	0.0	0.2		
								$[NH_4^+]$	4.2	7.0	0.0	0.0		
								$[Cl^-]$	0.5	0.0	0.4	2.1		
								$[NO_3^-]$	0.1	0.0	2.3	1.4		
								$[nss\text{-}SO_4^{2-}]$	3.8	13.9	0.4	0.1		
9	3	22 Sep 8:43–21:42	2.0	28.2	75	0.3	34.5	$[Na^+]$	0.0	0.8	3.8	3.6	1.5	0.5
								$[Mg^{2+}]$	0.0	0.0	0.3	0.4		
								$[NH_4^+]$	4.4	23.5	0.0	0.2		
								$[Cl^-]$	0.0	0.1	0.8	2.5		
								$[NO_3^-]$	0.0	0.1	1.7	2.1		
								$[nss\text{-}SO_4^{2-}]$	5.8	58.8	1.0	0.4		
10	4	27 Sep 0:32–8:39	8.3	29.2	66	0.5	0.3	$[Na^+]$	0.0	6.2	43.6	83.9	17.8	12.5
								$[Mg^{2+}]$	0.0	0.5	5.1	10.2		
								$[NH_4^+]$	11.4	38.8	0.0	0.0		
								$[Cl^-]$	0.1	0.2	30.9	79.7		
								$[NO_3^-]$	0.1	0.1	13.0	15.1		
								$[nss\text{-}SO_4^{2-}]$	9.3	41.8	1.1	0.0		
11	4	27 Sep 8:57–22:01	7.1	28.5	70	0.5	1.2	$[Na^+]$	0.2	5.1	31.6	67.7	12.9	10.1
								$[Mg^{2+}]$	0.0	0.4	3.6	8.4		
								$[NH_4^+]$	4.9	26.7	0.0	0.0		
								$[Cl^-]$	0.2	0.1	21.7	62.9		
								$[NO_3^-]$	0.1	0.1	10.7	12.9		
								$[nss\text{-}SO_4^{2-}]$	4.6	28.7	0.8	0.4		

Table 1. (continued)

SN	Leg	Time	WS, m/s	Temp., °C	RH, %	$[HNO_3]$ nmol/m^3	$[SO_2]$ nmol/m^3	Concentrations, nmol/m^3 Size Range, μm	<0.2	0.2–2	2–8	>8	A, mm^2/m^3 2–8	>8
12	4	27 Sep 22:18–28 Sep 8:40	11.0	27.0	77	0.6	0.8	$[Na^+]$	0.1	8.3	49.7	354	20.3	52.7
								$[Mg^{2+}]$	0.0	0.6	6.6	42.5		
								$[NH_4^+]$	1.7	11.0	0.0	0.0		
								$[Cl^-]$	0.1	0.1	49.0	399		
								$[NO_3^-]$	0.1	0.1	6.1	2.9		
								$[nss\text{-}SO_4^{2-}]$	2.3	16.4	0.0	0.0		
13	4	28 Sep 9:00–21:51	12.8	24.5	75	1.5	4.5	$[Na^+]$	1.3	5.6	37.7	272	15.4	40.4
								$[Mg^{2+}]$	0.0	0.3	4.2	32.2		
								$[NH_4^+]$	8.0	39.5	0.1	0.4		
								$[Cl^-]$	1.2	0.1	25.3	296		
								$[NO_3^-]$	0.1	0.4	14.6	13.4		
								$[nss\text{-}SO_4^{2-}]$	5.5	40.3	1.1	1.3		
14	4	28 Sep 22:06–29 Sep 4:38 21:51	4.4	23.6	61	4.4	43.7	$[Na^+]$	0.4	2.5	11.4	19.4	4.7	2.9
								$[Mg^{2+}]$	0.0	0.0	1.3	2.3		
								$[NH_4^+]$	19.0	55.8	0.9	0.5		
								$[Cl^-]$	0.2	0.4	1.7	14.6		
								$[NO_3^-]$	0.5	4.2	11.8	8.2		
								$[nss\text{-}SO_4^{2-}]$	10.8	29.2	0.8	0.6		

[a]SN and Leg respectively denote the sample and Leg number. WS and RH are the average wind speed and relative humidity during the sampling. A is the surface area of aerosol particles in 2–8 and >8 μm size ranges estimated from the geometric mean diameter of 4 and 11 μm.

Japan resemble those of values reported by *Nakamura et al.* [2005] and *Shiobara et al.* [2007].

3.3. Modification of Sea Salt Aerosols

3.3.1. Cl^- Deficiency in Coarse SSA Particles

[15] Figure 5 shows scatterplots of Cl^- and Mg^{2+} versus the Na^+ concentration in size-segregated coarse particles (>8 μm and 2–8 μm). Concentrations of Mg^{2+} in both size ranges (Figures 5a and 5b) were correlated well with Na^+ concentration. Molar ratios of Mg^{2+}/Na^+ in both size ranges were similar to the molar ratio (0.11) in seawater [*Wilson*, 1975]. The correlation of the concentrations and their molar ratio suggest that Na^+ and Mg^{2+} were derived mainly from seawater. The Cl^- concentration for particles of >8 μm (Figure 5c) was correlated well with Na^+ concentrations, but some samples showed slightly lower values to the seawater ratio (1.16). Furthermore, all Cl^- concentrations in the 2–8 μm range (Figure 5d) showed lower values to the seawater ratio, implying a Cl^- deficiency in samples.

[16] Figure 6 presents the amount of Cl^- deficiency (ΔCl^-, circles) and a stacked bar plot of NO_3^- and nss-SO_4^{2-} in size-segregated coarse particles, all in equivalent concentrations. Amounts of Cl^- deficiency (ΔCl^-) from the seawater composition were estimated from Na^+ concentrations in the sample and the Cl^-/Na^+ equivalent ratios in the seawater [*Wilson*, 1975] using the following equations.

$$[\Delta Cl^-] = [\text{sea} - \text{salt(ss)}Cl^-] - [Cl^-]_{obs} = 1.16[Na^+]_{obs} - [Cl^-]_{obs} \quad (4)$$

Most ΔCl^- concentrations presented in Figure 6 were nearly equal to the sum of NO_3^- and nss-SO_4^{2-} concentrations in the samples, which suggests that the Cl^- that originally existed in SSA particles was displaced by acidic components such as HNO_3 and SO_2.

$$HNO_3 + NaCl \rightarrow NaNO_3 + HCl \uparrow \quad (5)$$

$$H_2SO_4(\text{from oxidation of } SO_2) + 2NaCl \rightarrow Na_2SO_4 + 2HCl \uparrow \quad (6)$$

[17] Because the NO_3^-/Na^+ concentration ratio in surface seawater is <0.001 [*James*, 2005], high NO_3^-/Na^+ ratios (0.01–1.03) observed in coarse particles suggest that most of the NO_3^- in coarse particles was added from the atmosphere and derived from nonsea-salt compounds [*Parungo et al.*, 1986; *Mamane and Mehler*, 1987; *Pósfai et al.*, 1995; *Hara et al.*, 1999; *Zhuang et al.*, 1999; *Pryor and Sørensen*, 2000]. Similarly, absorption and subsequent oxidation of SO_2 injects additional SO_4^{2-} to coarse SSA particles as nss-SO_4^{2-} [*Okada et al.*, 1978; *Parungo et al.*, 1986; *McInnes et al.*, 1994; *Pósfai et al.*, 1995; *Buseck and Pósfai*, 1999].

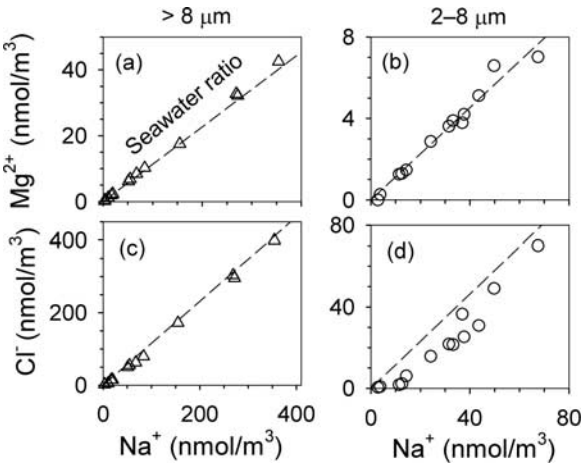

Figure 5. Scatterplots of Mg^{2+} (a and b) and Cl^- (c and d) versus Na^+ concentration in size-segregated coarse particles (a and c, >8 μm; b and d, 8–2 μm). Dashed lines in figures indicate molar ratios (0.11 for Mg^{2+}/Na^+ and 1.16 for Cl^-/Na^+) in seawater [*Wilson*, 1975].

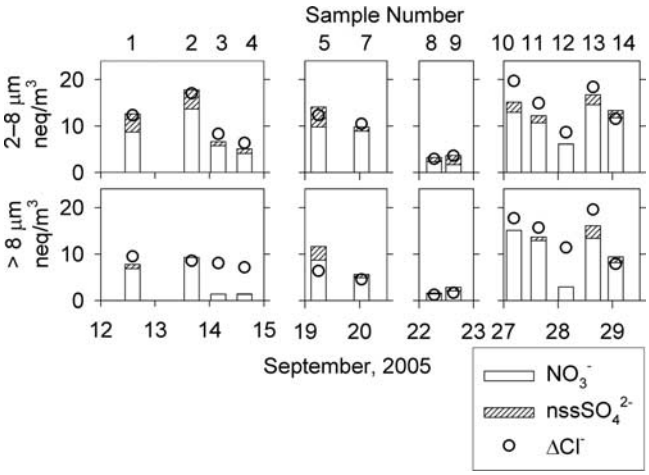

Figure 6. Amounts of Cl^- deficiency (ΔCl^-, circles; deficit from seawater composition inferred from $1.16 \times Na^+$ concentration) and stacked bar plots of NO_3^- and nss-SO_4^{2-} in size-segregated coarse particles, all in equivalent concentrations (neq m^{-3}). Numbers shown at the top of panel correspond to the sample numbers shown in Figure 3 and Table 1. Upper and lower panels respectively represent 2–8 μm and >8 μm size ranges.

Although the HNO_3 concentration in the atmosphere was almost the same or lower than SO_2, the NO_3^- concentration found in coarse particles was more than four times higher than that of nss-SO_4^{2-} in most samples (Figure 4). Higher particulate NO_3^- than nss-SO_4^{2-} concentration in coarse SSA particles is presumably attributable to factors which might include the relatively slow oxidation process of SO_2 to yield nss-SO_4^{2-} inside SSA particles, which is a multistep process with strong pH dependency [*Keen et al.*, 1998]. Another factor might be the difference of uptake coefficients for HNO_3 and SO_2 on SSA particles. In laboratory studies, *Gebel et al.* [2000] pointed out the initial uptake coefficient of SO_2 was as high as 0.09 for humid synthetic sea salt coarse particles, but the coefficient rapidly decreased below 0.01, as expected for approaching the equilibrium saturation concentration in an aqueous solution in SSA particles. On the other hand, the respective net uptake coefficients of HNO_3 were suggested for 0.1 and 0.03 for NaCl particles of 2 μm and 15 μm diameters [*Liu et al.*, 2007]. The wide ranges of the uptake coefficient for HNO_3 and SO_2, which have been reported in the literature [*Rossi*, 2003], suggest the complexity of heterogeneous reactions on SSA particles. Our results imply that the uptake coefficient of HNO_3 is larger than that of SO_2 for coarse SSA particles under real atmospheric conditions with low gaseous concentrations.

[18] For the >8 μm diameter particles in samples 3, 4, and 12, the ΔCl^- concentrations were higher than the sum of NO_3^- and nss-SO_4^{2-} concentrations. $CH_3SO_3^-$ and F^- were not detected in those samples. The respective sums of CH_3COO^- and $HCOO^-$ concentrations were 0.6, 2.7, and 1.0 for samples 3, 4, and 12, which is much lower than the difference between ΔCl^- and the sum of NO_3^- and nss-SO_4^{2-} concentrations. A similar excess Cl^- depletion that is unexplained by NO_3^- and nss-SO_4^{2-} has been reported for SSA particles at a coastal site [*Yao et al.*, 2001].

3.3.2. Factors Controlling Modification of SSA Particles

[19] Figure 7a depicts a scatterplot of the size-segregated Na^+ concentration and wind speed, indicating increased Na^+ concentration with increasing wind speed, which is especially apparent for the >8 μm range. Figure 7b presents the Na^+ concentration ratio ($Na^+_{2-8}/Na^+_{>8}$) of 2–8 μm to >8 μm size ranges versus wind speed. The $Na^+_{2-8}/Na^+_{>8}$ ratio shows a clear decrease with increasing wind speed, which is consistent with production of more numerous coarse SSA particles from the sea surface under the stronger wind conditions, which is well known as the exponential increase of SSA mass concentration with wind speed [*Lewis and Schwartz*, 2004].

[20] Figure 7c presents size-segregated concentration ratios of $\Delta Cl^-/ssCl^-$ versus wind speed. Most of the $\Delta Cl^-/ssCl^-$ ratios for fine particles (0.2–2 μm) are greater than 0.8 and are mostly close to unity, suggesting that almost all $ssCl^-$ are depleted, irrespective of wind speed. In contrast, the $\Delta Cl^-/ssCl^-$ ratios for coarse particles decrease with increasing wind speeds with a higher degree of depletion for the 2–8 μm size range than for those which are >8 μm. A similar tendency of the size dependency on the $\Delta Cl^-/ssCl^-$

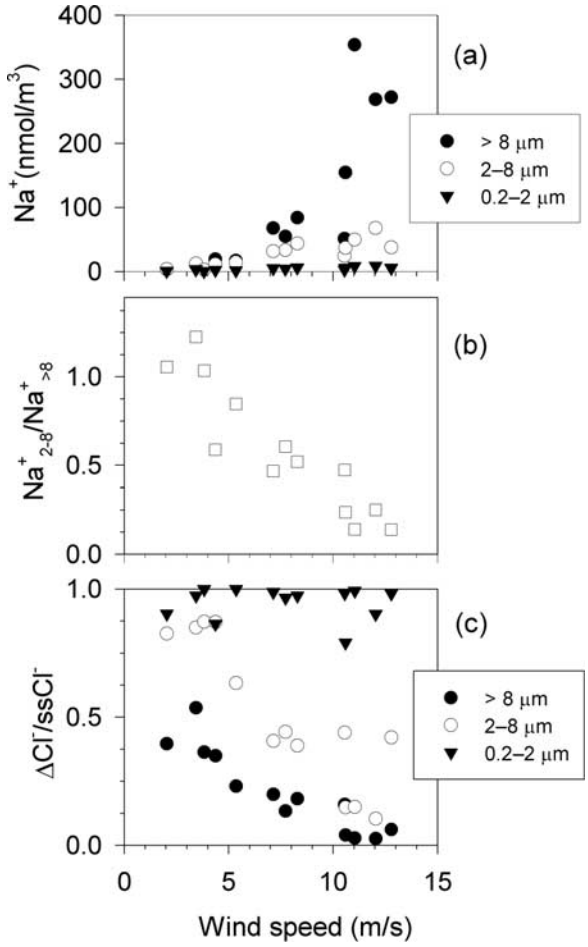

Figure 7. Relationship between (a) size-segregated Na^+ concentration versus wind speed, (b) Na^+ concentration ratio ($Na^+_{2-8}/Na^+_{>8}$) for the 2–8 μm to 8 μm size ranges versus wind speed, and (c) size-segregated $\Delta Cl^-/ssCl^-$ versus wind speed.

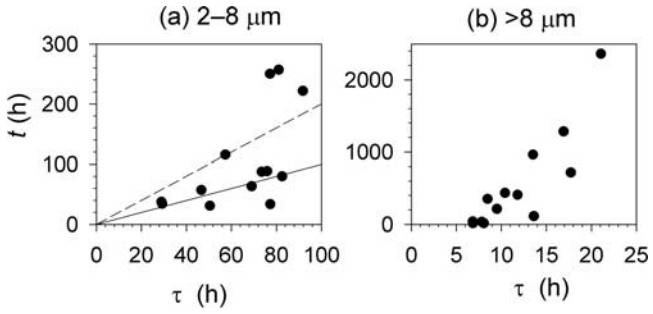

Figure 8. Scatterplots of the time (t) required for accumulating NO_3^- concentration based on HNO_3 gas concentration versus τ for the falling time from 500 m altitude: (a) for 2–8 μm and (b) for >8 μm size ranges. Solid and dotted lines in Figure 8a respectively represent τ = t and $2\tau = t$.

ratios has been reported in the literature [*Pakkanen*, 1996; *Yao et al.*, 2003]. The deposition velocity of larger SSA particles is much higher than that of smaller SSA particles. Therefore the residence time in air will be shorter in larger SSA particles. For example, assuming that the mixing layer height is 500 m and that the RH of air is 80% under the condition of wind speed of 10 m/s at 10 m height, values of residence times of SSA particles with 4 μm and 10 μm diameter are estimated respectively as 2.3 d and 10 h [*Lewis and Schwartz*, 2004]. As discussed in greater detail later, the difference in residence time might cause a difference in the $\Delta Cl^-/ssCl^-$ ratios and amounts of NO_3^- and nss-SO_4^{2-} accumulated on SSA particles.

[21] On the other hand, the amount of $\Delta Cl^-/ssCl^-$ in the >8 μm range is very low (<0.1) for wind speeds greater than 10 m/s (Figure 7c). Inertial impaction for the deposition velocity increases with increasing wind speed. Its contribution to overall V_{dry} is greater for >8 μm than that for the 2–8 μm size range. Considering the shorter residence time of coarser SSA particles (such as >8 μm) under strong winds, SSA particles of >8 μm under wind conditions of >10 m/s might not have sufficient time to accumulate NO_3^-. Consequently, as a first approximation assuming constant precursor concentrations, wind speed and particle size are the major controlling factors on the $\Delta Cl^-/ssCl^-$ ratio because of the difference of residence time of SSA particles in marine air to accumulate NO_3^- and nss-SO_4^{2-}.

[22] As portrayed in Figure 6, modification of SSA particles was dominated by NO_3^-. We will discuss the relationship between the time required for accumulating NO_3^- and the residence time of SSA particles using a simple uptake model [*Hara et al.*, 1999] to further explore the modification processes of SSA particles by NO_3^-. Assuming a steady state condition of NO_3^- formation on the SSA particle surfaces, the heterogeneous production rate ($d[NO_3^-]/dt$ (nmol/m^{3}s)) is given as

$$\frac{d[NO_3^-]}{dt} \frac{\gamma A v}{4}[HNO_3] \tag{7}$$

where γ is the reactive uptake coefficient, A is the surface area for aerosols per cubic meter of air (Table 1), and v is the mean molecular speed. Assuming that all Na^+ found in coarse particles originated from seawater, the Na^+ concentration and geometric mean diameter for the size range sampled were used to estimate A in each size-segregated bin. Namely, A is calculated as

$$A = 4\pi\left(\frac{d_{RH80}}{2}\right)^2 n, \tag{8}$$

where d_{RH80} refers to the diameter of a SSA particle in equilibrium with the atmosphere at 80% RH, and n is the number concentration of SSA particles in a cubic meter of air. Also, n is

$$n = \frac{3.26 \times [Na^+]}{m_{dry}}, \tag{9}$$

where m_{dry} is the dry sea salt mass and the coefficient of 3.26 represents the mass ratio of sea salt to Na^+ [*Lewis and Schwartz*, 2004]. In addition, d_{RH80} is almost twice the equivalent dry diameter of SSA particles [*Tang et al.*, 1997]. Therefore the dry sea salt mass (m_{dry}) of seawater droplet at RH 80% is expressed as

$$m_{dry} = \frac{4\pi}{3}\rho_{dry}\left(\frac{d_{RH80}}{4}\right)^3, \tag{10}$$

where ρ_{dry} (2.2 g cm^{-3}) is the density of dry sea salt [*Lewis and Schwartz*, 2004]. Although minor reactive nitrogen oxides might be involved in NO_3^- formation of SSA particles in the marine boundary layer, we assume that the sole predominant precursor forming NO_3^- in coarse SSA particles is HNO_3 and that its gaseous concentration is constant during modification of SSA particles. Finally, the NO_3^- concentration accumulated on SSA particles can be estimated using the following equation.

$$[NO_3^-] = \frac{\gamma v}{4} A t [HNO_3] \tag{11}$$

In that equation, t is the time to accumulate NO_3^- in SSA particles. To estimate the range of t required for accumulating NO_3^- concentration observed, γ is used respectively 0.02 and 0.06 for particles of 4 μm and 11 μm [*Liu et al.*, 2007].

[23] The residence time (τ) is simply assumed as the time necessary for falling from 500 m altitude (as a minimum height of the marine boundary layer) at the dry deposition velocity, depending on wind speed and particle size.

$$\tau = \frac{500}{V_{dry-p}} \tag{12}$$

In that equation, $V_{dry\text{-}p}$ is dry deposition velocity of SSA particles. Note that τ estimated here must be considered as the minimum because of simplification for considering only downward movement and using a fixed minimum height of the marine boundary layer.

[24] Figure 8 shows the size-dependent scatterplots of the time (t) required for accumulating NO_3^- concentration based

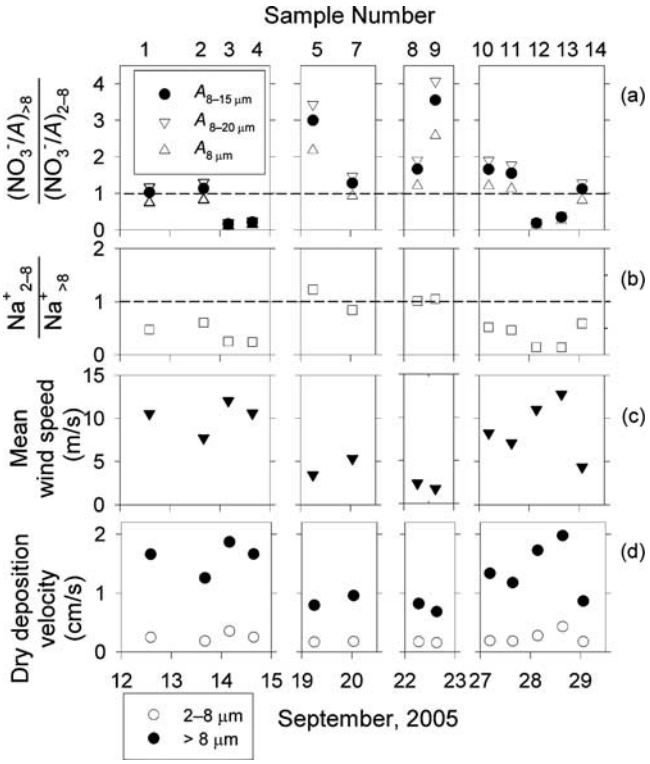

Figure 9. (a) Ratio of NO_3^- concentration per unit area (NO_3^-/A) (filled circles) for the 2−8 μm and >8 μm size ranges with maximum and minimum estimations (up and down open triangles). (b) Na^+ concentration ratio in 2−8 μm and >8 μm size ranges. (c) Mean wind speed during aerosol sampling. (d) Dry deposition velocity for geometric mean diameters (4 μm and 11 μm) of the respective size ranges. Filled circles in Figure 9a were calculated from A using geometric mean diameters of 4 μm and 11 μm. Open (up and down) triangles in Figure 9a were calculated from A using different geometric mean diameters for the larger size range as 13 μm and 8 μm, respectively (see text).

on HNO_3 gas concentration observed versus τ for the falling time from 500 m altitude. In Figure 8a, the solid line represents τ = t and the dotted line shows the case of $2\tau = t$. For the size range of 2−8 μm (Figure 8a), most plots are below the dotted line (2τ), suggesting that NO_3^- accumulation occurs during the residence time in the air. However, for the size range of >8 μm (Figure 8b), τ is more than one order lower than that of t. That large discrepancy is enigmatic, but errors might arise from: (1) the assumption of constant HNO_3 gaseous concentration during modification; (2) uncertainty of γ for HNO_3 in clean atmospheric conditions, especially for SSA particles with >8 μm size range; and (3) estimation of $V_{dry\text{-}p}$ for the >8 μm size range. Although we examined $V_{dry\text{-}p}$ using a different upper limit for the sampling, the large discrepancy was unchanged.

[25] As described earlier, the residence time of SSA particles in the marine boundary layer depends on their size and meteorological situation: faster deposition occurs for larger particles and for strong wind conditions because of gravitational settling and inertial impaction onto the sea surface, suggesting lower (higher) NO_3^- accumulation in larger (smaller) SSA particles. On the other hand, the total surface area of particles per unit SSA mass increases with decreasing particle diameter. As shown in equation (11), the NO_3^- concentration on SSA particles is related directly to A, suggesting that the accumulated NO_3^- per unit mass of SSA particles might also increase with decreasing particle size during the initial stage of modification.

[26] The NO_3^- concentrations per unit area (NO_3^-/A) of SSA particles are estimated using NO_3^- concentrations and the A for the size ranges of 2−8 μm and >8 μm (Figure 9a). In Figure 9a, the dotted line shows that NO_3^-/A_{2-8} is equal to $NO_3^-/A_{>8}$; upright and reversed triangles represent the values using A for two kinds of geometric mean diameter (13 μm for 8−20 μm and 8 μm as the lowest). These triangles represent the range of estimation for the varying upper limit of aerosol sampling. Figure 9b shows the Na^+ concentration ratio ($Na^+_{2-8}/Na^+_{>8}$) of 2−8 μm to >8 μm size ranges. Figure 9c shows the mean wind speed during aerosol sampling. As discussed for Figure 7b, high (low) $Na^+_{2-8}/Na^+_{>8}$ ratios correspond to low (high) wind speeds. Figure 9d shows the dry deposition velocity for geometric mean diameters (4 μm and 11 μm) of the size ranges collected, as estimated from the model by *Lewis and Schwartz* [2004] with the mean wind speed.

[27] In Figure 9a, the ratios of $NO_3^-/A_{>8}$ to NO_3^-/A_{2-8} are divided into three groups: low ratios (<0.5) for samples 3, 4, 12, and 13; high ratios (>2.0) for samples 5 and 9; and ratios near unity for samples 1, 2, 7, and 14. Members of these three groups were unchanged despite consideration of different A for various upper size limits. For the samples of low ratios, values of the mean wind speed were higher than ca. 10 m/s. Under strong wind conditions, the production rate of coarser SSA particles, such as those >8 μm, is expected to be high. In addition, coarser SSA particles in the marine boundary layer are deposited rapidly back to the sea surface because of their higher dry deposition velocity. Because of the shorter residence time of SSA particles within the marine boundary layer, less NO_3^- accumulates on coarser SSA particles such as >8 μm, which is consistent with observed lower ratios of $NO_3^-/A_{>8}$ to NO_3^-/A_{2-8}.

[28] For samples with high ratios, the values of mean wind speed were low (<3.5 m/s). Under low wind conditions, the production rate of SSA particles was low and the concentration ratio of $Na^+_{2-8\mu m}/Na^+_{8\mu m}$ is high (Figure 7b), but the residence time of SSA particles is longer because of the lower dry deposition velocities. As presented in Figure 7c, 80% of $ssCl^-$ of SSA particles with 2−8 μm were displaced under low wind conditions, implying that the residence time of 2−8 μm SSA particles was longer than the time for displacing most $ssCl^-$ after accumulation of NO_3^-. This result is consistent with the analysis discussed in Figure 8a. On the other hand, a sea salt aerosol particle with >8 μm diameter can hold greater amounts of NO_3^- than one with 2−8 μm diameter because the volume to surface area ratio is much larger for a >8 μm particle than a particle of 2−8 μm diameter. That inference is consistent with observed higher ratios of $NO_3^-/A_{>8}$ to NO_3^-/A_{2-8} under low wind conditions. For the samples with ratios near unity, the values of mean wind speed were 4−11 m/s. A ratio of unity implies that NO_3^- is equally accumulated on SSA particles, as though modification by NO_3^- is limited to the thin surface of SSA particles independently of size.

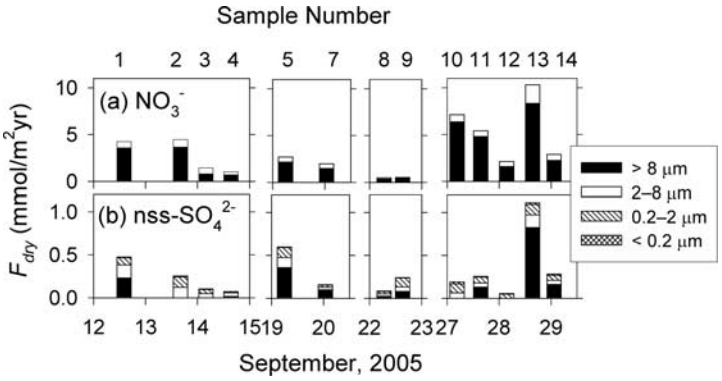

Figure 10. Dry deposition flux of aerosol particles ($F_{\text{dry-}p}$) estimated for (a) NO_3^- and (b) nss-SO_4^{2-}.

[29] In summary, the amount of NO_3^- accumulated on SSA particles might depend on the residence time, but the amount is also limited by the SSA particle size.

3.4. Dry Deposition Flux of NO_3^- and nss-SO_4^{2-}

[30] Dry deposition flux ($F_{\text{dry-p}}$) of NO_3^- and nss-SO_4^{2-} in aerosol particles was estimated using equation (1). Parameters in the estimates are given as dry deposition velocities of aerosol particles (Figure 9c, $V_{\text{dry-}p}$) and chemical data (Figure 4). Values of $V_{\text{dry-}p}$ for coarse particles (>2 μm, Figure 9c) are greater than 0.1 cm/s, but those for fine particles (<2 μm, not shown) are less than 0.01 cm/s. Consequently, $F_{\text{dry-}p}$ depends not only on the total concentration of the aerosol phase but also on its size distribution.

[31] Figure 10 shows results of $F_{\text{dry-p}}$ estimated for NO_3^- and nss-SO_4^{2-}. The range of $F_{\text{dry-p}}$ for NO_3^- was from 0.5–10 mmol/m^2 a; that of nss-SO_4^{2-} was 0.05–1.1 mmol/m^2 a. The maximum $F_{\text{dry-}p}$ for both ions was observed for sample 13, which showed high ionic concentration in coarse aerosols with high $V_{\text{dry-}p}$ under strong wind conditions. As described earlier, the size distribution of aerosols is an important factor for $F_{\text{dry-}p}$. For example, $F_{\text{dry-}p}$ of NO_3^- for coarse particles accounts for 99–100% of the total $F_{\text{dry-}p}$ of NO_3^-. Among them, 78% of $F_{\text{dry-}p}$ is of the size range of >8 μm. Although NO_3^- was observed to have comparable concentration for 2–8 μm (8.3 nmol/m^3) and >8 μm (6.7 nmol/m^3) size ranges, $F_{\text{dry-}p}$ (2.7 mmol/m^2 a) for >8 μm was much larger than that (0.6 mmol/m^2 a) of 2–8 μm because $V_{\text{dry-p}}$ for >8 μm was about eight times larger than that of 2–8 μm, on average.

[32] Another example of the effects of size distribution is apparent in nss-SO_4^{2-} flux. Although the concentration of nss-SO_4^{2-} in the fine mode (35.6 nmol/m^3) was much higher than that (1.9 nmol/m^3) of the coarse mode, the $F_{\text{dry-}p}$ of coarse nss-SO_4^{2-} mode contributed a large fraction (63% on the average) of the total flux.

[33] Figure 11 shows the dry deposition flux of aerosol particles ($F_{\text{dry-}p}$ for NO_3^- and nss-SO_4^{2-}) and gases ($F_{\text{dry-}g}$ for HNO_3 and SO_2). The median value of $F_{\text{dry-}p}$ (2.4 mmol/m^2 a) for NO_3^- was about one order higher than the $F_{\text{dry-}g}$ (0.15 mmol/m^2 a) of HNO_3, although the median value of $F_{\text{dry-}p}$ (0.25 mmol/m^2 a) for nss-SO_4^{2-} was almost the same as $F_{\text{dry-}g}$ (0.28 mmol/m^2 a) of SO_2. In coastal areas of the US, F_{dry} of NO_3^- and HNO_3 show no large difference: $F_{\text{dry-}g}$ was slightly larger than $F_{\text{dry-}p}$ for pollution-affected cases [*Russell et al.*, 2003; *Fischer et al.*, 2006]. Those studies were made in coastal areas. For that reason, high HNO_3 concentrations (23 nmol/m^3 as a median value) were frequently observed. In this study, a high HNO_3 concentration (4.4 nmol/m^3) was also found in the Seto Inland Sea area, but the HNO_3 concentrations for the remaining samples were below 1.6 nmol/m^3. The low HNO_3 concentration over the oceanic region might promote small $F_{\text{dry-}g}$ relative to $F_{\text{dry-}p}$ for nitrate. For the phase partitioning of SO_2 and nss-SO_4^{2-}, one order larger F_{dry} for SO_2 was reported for the eastern Mediterranean [*Kouvarakis et al.*, 2002]. In their results, SO_2 concentrations were nearly equal to nss-SO_4^{2-}, which is also different from this study.

4. Summary and Conclusions

[34] Samples of size-segregated aerosol particles and acidic gases were obtained on board during 12–29 September 2005 over the ocean around the western part of the Japanese Islands. Results of chemical analyses of the samples indicated that coarse (>2 μm diameter) aerosol particles were mostly sea salt aerosol particles (SSA particles). For coarse SSA particles, the concentration of the Cl^- deficiency (ΔCl^-, estimated from Cl^-/Na^+ ratios in the seawater and Na^+ concentration in the sample) was comparable to the sum of the equivalent concentrations of NO_3^- and nonsea-salt (nss) SO_4^{2-}, which suggests that Cl^-

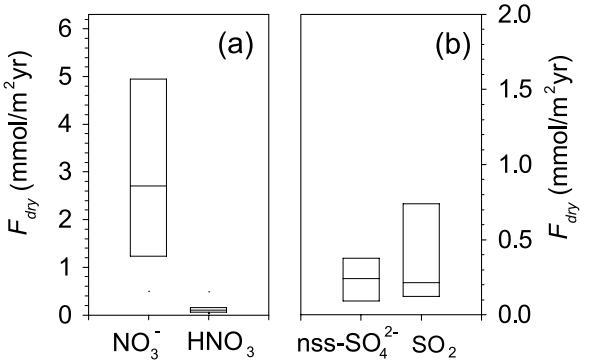

Figure 11. Dry deposition flux of aerosol particles and gases estimated for samples in this study. The boundaries of the boxes closest to and most distant from zero respectively indicate the 25th and 75th percentiles. Thin horizontal lines within the boxes represent the respective median values.

in coarse SSA particles was displaced by acidic gases such as HNO_3 and SO_2. Ratios of ΔCl^-/sea salt Cl^- for three size ranges versus wind speed indicated that the modification degree of SSA particles tended to differ with the size range and wind speed: almost complete displacement occurred, irrespective of wind speed, for the fine 0.2–2 μm range. A lesser degree of modification occurred with increasing wind speed for sizes of 2–8 μm, and a similar but lesser degree of modification occurred with nearly no modification above 10 m/s for the >8 μm range. On the basis of discussion of the deposition velocity of SSA particles in the marine boundary layer, at a first approximation assuming constant precursor concentrations, wind speed and particle size are suggested as major controlling factors of the ΔCl^-/ssCl^- ratio through the difference of residence time of SSA particles and accumulation of NO_3^- and nss-SO_4^{2-}. Ratios of the NO_3^- concentration per unit surface area for 2–8 μm and >8 μm size ranges were compared with wind speed conditions to elucidate SSA modification by NO_3^-. Under high (low) wind conditions, the NO_3^- concentration per unit surface area was lower (higher) in the >8 μm range than in the 2–8 μm range. Because the residence time of SSA particles in the marine boundary layer might depend on its size and wind speed, higher (lower) wind conditions might engender a lower (higher) degree of SSA modification by HNO_3.

[35] The concentration of NO_3^- in coarse particles was more than four times higher than that of nss-SO_4^{2-}, although the concentration of HNO_3 in the atmosphere was almost equal to that of SO_2. The respective dry deposition fluxes (F_{dry}) of NO_3^-, nss-SO_4^{2-}, HNO_3, and SO_2 were estimated by considering the wind speed and aerosol particle size. On the average, F_{dry} of particulate NO_3^- was 10 times larger than that of HNO_3, although F_{dry} of nss-SO_4^{2-} was almost equal to that of SO_2, which underscores the different phase partitioning from results of coastal area examinations reported in the literature.

[36] **Acknowledgments.** Aerosol measurements made on board the R/V *Shirase* were carried out as part of the JARE 47 Training Cruise Program operated by the Japan Defense Agency. We especially thank the JARE 47 Team and the crew of R/V *Shirase* for their support with the onboard aerosol measurement program. The authors gratefully acknowledge the NOAA Air Resources Laboratory (ARL) for providing the HYSPLIT transport model website (http://www.arl.noaa.gov/ready.html) described herein. This work was performed with the support of a Grant-in-Aid for Scientific Research in Priority Areas, grant 14048228 (AIE) and 18067005 (W-PASS), provided by the Ministry of Education, Culture, Sports, Science and Technology, Japan, and by Grants-in-Aid for Scientific Research (B) 15310012 from the Ministry of Education, Culture, Sports, Science and Technology. This research is a contribution to the IGBP/SOLAS activity.

References

Akimoto, H. (2003), Global air quality and pollution, *Science*, *302*, 1716–1719.

Andreae, M. O. (1995), Climatic effects of changing atmospheric aerosol levels, in *Future Climates of the World: A Modeling Perspective. World Survey of Climatology*, vol. 16, edited by A. Henderson-Sellers, pp. 347–398, Elsevier, Amsterdam.

Buseck, P. R., and M. Pósfai (1999), Airborne minerals and related aerosol particles: Effects on climate and the environment, *Proc. Natl. Acad. Sci. U.S.A.*, *96*, 3372–3379.

Chen, Y., S. Mills, J. Street, D. Golan, A. Post, M. Jacobson, and A. Paytam (2007), Estimates of atmospheric dry deposition and associated input of nutrients to Gulf of Aqaba seawater, *J. Geophys. Res.*, *112*, D04309, doi:10.1029/2006JD007858.

Draxler, R. R., and G. D. Rolph (2003), HYSPLIT (Hybrid Single-Particle Lagrangian Integrated Trajectory) model access via NOAA ARL READY website, (http://www.arl.noaa.gov/ready/hysplit4.html), NOAA Air Resour. Lab., Silver Spring, Md.

Duce, R. A., et al. (1991), The atmospheric input of trace species to the world ocean, *Global Biogeochem. Cycles*, *5*, 193–259.

Fischer, E., A. Pszenny, W. Keene, J. Maben, A. Smith, A. Stohl, and R. Talbot (2006), Nitric acid phase partitioning and cycling in the New England coastal atmosphere, *J. Geophys. Res.*, *111*, D23S09, doi:10.1029/2006JD007328.

Fujita, S., Y. Tonooka, and K. Ohta (1992), Annual contribution of volcanic sulfur dioxide emissions to the atmosphere in Japan, *J. Jpn. Soc. Air Pollut.*, *27*, 336–343.

Galloway, G. N., and E. B. Cowlling (2002), Reactive nitrogen and the world, 200 years of change, *Ambio*, *31*, 64–71.

Gebel, M. E., B. Finlayson-Pitts, and J. A. Ganske (2000), The uptake of SO_2 on synthetic sea salt and some of its components, *Geophys. Res. Lett.*, *27*, 887–890.

Hangal, S., and K. Willeke (1990), Overall efficiency of tubular inlets sampling at 0–90 degrees from horizontal aerosol flows, *Atmos. Environ.*, *24A*, 2379–2386.

Hara, K., K. Osada, M. Hayashi, K. Matsunaga, T. Shibata, Y. Iwasaka, and K. Furuya (1999), Fractionation of inorganic nitrates in winter Arctic troposphere: Coarse aerosol particles containing inorganic nitrates, *J. Geophys. Res.*, *104*, 23,671–23,679.

He, Y., I. Uno, Z. Wang, T. Ohara, N. Sugimoto, A. Shimizu, A. Richter, and J. P. Burrows (2007), Variations of the increasing trend of tropospheric NO_2 over central east China during the past decade, *Atmos. Environ.*, *41*, 4865–4876.

Hinds, C. H. (1999), Straight-line acceleration and curvilinear particle motion, in *Aerosol Technology*, 2nd ed., pp. 111–140, John Wiley, Onc.

James, R. (2005), *Marine Biogeochemical Cycles*, 2nd ed., 130 pp., The Open Univ., Elsevier.

Keen, W. C., R. Sander, A. A. P. Pszenny, R. Vogt, P. J. Crutzen, and J. N. Galloway (1998), Aerosol pH in the marine boundary layer: A review and model evaluation, *J. Aerosol Sci.*, *29*, 339–356.

Kouvarakis, G., H. Bardouki, and N. Mihalopoulos (2002), Sulfur budget above the Eastern Mediterranean: Relative contribution of anthropogenic and biogenic sources, *Tellus*, *54B*, 201–212.

Lewis, E. R. and S. E. Schwartz (2004), Sea salt aerosol production: Mechanisms, methods, measurement and model–A critical review, *Geophys. Monogr.*, vol. 152, 413 pp., AGU, Washington, D. C.

Lindfors, V., S. M. Joffre, and J. Damski (1993), Meteorological variation of the wet and dry deposition of sulphur and nitrogen compounds over the Baltic Sea, *Water Air Soil Pollut.*, *66*, 1–28.

Liu, Y., J. P. Chain, H. Wang, and A. Laskin (2007), Kinetic study of heterogeneous reaction of deliquesced NaCl particles with gaseous HNO_3 using particle-on-substrate stagnation flow reactor approach, *J. Phys. Chem. A*, *111*, 10,026–10,043.

Mamane, Y., and M. Mehler (1987), On the nature of nitrate particles in a coastal urban area, *Atmos. Environ.*, *21*, 1989–1994.

Mark, D. (1998), Atmospheric aerosol sampling, in *Atmospheric Particles*, edited by R. M. Harrison and R. V. Grieken, pp. 29–94, John Wiley & Sons, Chichester England.

McInnes, L. M., D. S. Covert, P. K. Quinn, and M. S. Germani (1994), Measurements of chloride depletion and sulfur enrichment in individual sea-salt particles collected from the remote marine boundary layer, *J. Geophys. Res.*, *99*, 8257–8268.

Nakamura, T., K. Matsumoto, and M. Uematsu (2005), Chemical characteristics of aerosol transported from Asia to the East China Sea: An evaluation of anthropogenic combined nitrogen deposition in autumn, *Atmos. Environ.*, *39*, 1749–1758.

Ohara, T., H. Akimoto, J. Kurokawa, N. Horii, K. Yamaji, and T. Hayasaka (2007), An Asian emission inventory of anthropogenic emission sources for the period 1980–2020, *Atmos. Chem. Phys.*, *7*, 4419–4444.

Okada, K., Y. Ishizaka, T. Masuzawa, and K. Isono (1978), Chlorine deficiency in coast aerosols, *J. Meteorol. Soc. Jpn.*, *56*, 501–507.

Osada, K., M. Kido, C. Nishita, K. Matsunaga, Y. Iwasaka, M. Nagatani, and H. Nakada (2007), Temporal variation of water-soluble ions of free tropospheric aerosol particles over central Japan, *Tellus*, *59B*, 742–754.

Paerl, H. E. (1997), Coastal eutrophication and harmful algal blooms: Importance of atmospheric deposition and groundwater as "new" nitrogen and other nutrients sources, *Limnol. Oceanogr.*, *42*, 1154–1165.

Pakkanen, T. A. (1996), Study of formation of coarse particle nitrate aerosol, *Atmos. Environ.*, *30*, 2475–2482.

Parungo, F. P., C. T. Nagamoto, J. Rosinski, and P. L. Haagson (1986), A study of marine aerosols over the Pacific Ocean, *J. Atmos. Chem.*, *4*, 199–226.

Pio, C. A., and D. A. Lopes (1998), Chlorine loss from marine aerosol in a coastal atmosphere, *J. Geophys. Res.*, *103*, 25,263–25,272.

Pósfai, M., J. R. Anderson, P. R. Buseck, and H. Sievering (1995), Compositional variations of sea-salt-mode aerosol particles from the North Atlantic, *J. Geophys. Res.*, *100*, 23,063–23,074.

Pryor, S. C., and L. L. Sørensen (2000), Nitric acid sea salt reactions: Implications for nitrogen deposition to water surfaces, *J. Appl. Meteorol.*, *39*, 725–731.

Pryor, S. C., and L. L. Sørensen (2002), Dry deposition of reactive nitrogen to marine environments: Recent advances and remaining uncertainties, *Mar. Pollut. Bull.*, *44*, 1336–1340.

Richter, A., J. P. Burrows, H. Nüß, C. Granier, and U. Niemeier (2005), Increase in tropospheric nitrogen dioxide over China observed from space, *Nature*, *437*, 129–132.

Rossi, M. J. (2003), Heterogeneous reactions on salts, *Chem. Rev.*, *103*, 4823–4882.

Russell, K. M., W. C. Keene, J. R. Maben, J. N. Galloway, and J. L. Moody (2003), Phase partitioning and dry deposition of atmospheric nitrogen at the mid-Atlantic U.S. coast, *J. Geophys. Res.*, *108*(D21), 4656, doi:10.1029/2003JD003736.

Sievering, H., J. Boatman, M. Luria, and C. C. Van Valin (1989), Sulfur dry deposition over the western North Atlantic: The role of coarse aerosol particles, *Tellus*, *41B*, 338–343.

Shiobara, M., K. Hara, M. Yabuki, and H. Kobayashi (2007), Optical and chemical properties of marine boundary-layer aerosol around Japan determined from shipboard measurements in 2002, *Atmos. Environ.*, *41*, 4638–4652.

Slinn, S. A., and W. G. N. Slinn (1980), Predictions for particle deposition on natural waters, *Atmos. Environ.*, *14*, 1013–1016.

Spokes, L. J., S. G. Yeatman, S. E. Cornell, and T. D. Jickelles (2000), Nitrogen deposition to the eastern Atlantic Ocean: The importance of southeasterly flow, *Tellus*, *52B*, 37–49.

Streets, D. G., et al. (2003), An inventory of gaseous and primary aerosol emissions in Asia in the year 2000, *J. Geophys. Res.*, *108*(D21), 8809, doi:10.1029/2002JD003093.

Sugimoto, N., I. Matsui, A. Shimizu, I. Uno, K. Asai, T. Endoh, and T. Nakajima (2002), Observation of dust and anthropogenic aerosol plumes in the Northwest Pacific with a two-wavelength polarization lidar on board the research vessel Mirai, *Geophys. Res. Lett.*, *29*(19), 1901, doi:10.1029/2002GL015112.

Tang, I. N., A. C. Tridico, and K. H. Fung (1997), Thermodynamic and optical properties of sea salt aerosols, *J. Geophys. Res.*, *102*, 23269–23275.

Uno, I., M. Uematsu, Y. Hara, Y. J. He, T. Ohara, A. Mori, T. Kanaya, K. Murano, Y. Sadanaga, and H. Bandow (2007), Numerical study of the atmospheric input of anthropogenic total nitrate to the marginal seas in the western North Pacific region, *Geophys. Res. Lett.*, *34*, L17817, doi:10.1029/2007GL030338.

van der A, R. J., D. H. M. U. Peters, H. Eskes, K. F. Boersma, M. van Roozendael, I. De Smedt, and H. M. Kelder (2006), Detection of the trend and seasonal variation in tropospheric NO_2 over China, *J. Geophys. Res.*, *111*, D12317, doi:10.1029/2005JD006594.

Wilson, T. R. S. (1975), Salinity and the major elements of sea water, in *Chemical Oceanography 1*, 2nd ed., edited by J. P. Riley and G. Skirrow, pp. 365–413, Elsevier, New York.

Yao, X., M. Fang, and C. K. Chan (2001), Experimental study of the sampling artifact of Chloride depletion from collected sea salt aerosols, *Environ. Sci. Technol.*, *35*, 600–605.

Yao, X., M. Fang, and C. K. Chan (2003), The size dependence of chloride depletion in fine and coarse sea-salt particles, *Atmos. Environ.*, *37*, 743–751.

Yeatman, S. G., L. J. Spokes, and T. D. Jickells (2001), Comparisons of coarse-mode aerosol nitrate and ammonium at two polluted coastal sites, *Atmos. Environ.*, *35*, 1321–1335.

Zhang, J. (1994), Atmospheric wet deposition of nutrient elements: Correlation with harmful biological blooms in northwest Pacific coastal zones, *Ambio*, *23*, 468.

Zhuang, H., C. K. Chan, M. Fang, and A. S. Wexler (1999), Formation of nitrate and non-sea-salt sulfate on coarse particles, *Atmos. Environ.*, *33*, 4223–4233.

K. Hara, Faculty of Science, Fukuoka University, 8-19-1, Nanakuma, Jonan-ku, Fukuoka, 814-0180, Japan.

N. Kawakami, Aichi Environmental Research Center, 7-6 Nagare, Tsujimachi, Kita-ku, Nagoya, 462-0032, Japan.

H. Kobayashi, Interdisciplinary Graduate School of Medicine and Engineering, University of Yamanashi, 4-37, Takeda, Kofu 400-8510, Japan.

C. Nishita and K. Osada, Graduate School of Environmental Studies, Nagoya University, Furo-cho Chikusa-ku, Nagoya 464-8601, Japan. (kosada@nagoya-u.jp)

M. Shiobara and M. Yabuki, National Institute of Polar Research, 1-9-10, Kaga, Itabashi 173-8515, Japan.